

# Synthesis of Mesoporous Silica-Supported NiCo Bimetallic Nanocatalysts and Their Enhanced Catalytic Hydrogenation Performance

Jiajuan Li, Zizhu Wang, Yirui Ma, Caiyun Xu, and Shenghu Zhou\*

Cite This: *ACS Omega* 2023, 8, 12339–12347

Read Online

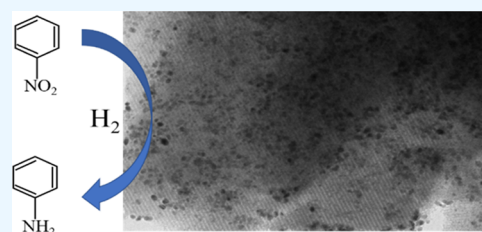
ACCESS |

Metrics &amp; More

Article Recommendations

Supporting Information

**ABSTRACT:** In this work, mesoporous silica SBA-16-supported NiCo bimetallic nanocatalysts were synthesized by coimpregnation of Ni and Co precursors followed by calcination and reduction, and various characterization techniques confirm the formation of NiCo bimetallic nanostructures in the catalysts. The synthesized NiCo/SBA-16 shows enhanced catalytic performance for hydrogenation of a series of nitroaromatics. Under the reaction conditions of 80 °C and 1.0 MPa of H<sub>2</sub>, the yields of aniline for nitrobenzene hydrogenation over NiCo<sub>0.3</sub>/SBA-16 can reach more than 99% at 2.0 h. The enhanced catalytic performance can be ascribed to the formation of NiCo bimetallic nanostructures, where the synergistic effect between Ni and Co improves their catalytic activities for hydrogenation of nitroaromatics.



## 1. INTRODUCTION

Aniline and its derivatives are very important chemicals used in the production of medicines, dyes, pigments, and pesticides.<sup>1–3</sup> With the increasing demands for aminoaromatics, their synthesis has attracted great attention in recent years.<sup>4</sup> Traditional production of aminoaromatics was achieved by the reduction of nitroaromatics with iron powders or hydrazine hydrate.<sup>5–7</sup> However, these two methods caused serious pollution to the environment. Currently, catalytic selective hydrogenation of nitroaromatics to aminoaromatics has received great attention because of their environmental friendliness and easy operation.<sup>8</sup> The hydrogenation of nitroaromatics can be carried out in the gas or liquid phase, and developing highly efficient catalysts is the key to promote this process.<sup>9–11</sup>

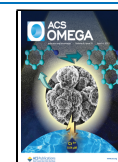
Noble metal catalysts, such as Pt,<sup>12,13</sup> Pd,<sup>14,15</sup> and Rh,<sup>16,17</sup> are generally considered to have strong activity for catalytic hydrogenation. For example, the two-dimensional metallic Pd nanosheet catalysts showed high nitrobenzene conversion as well as high aniline selectivity under 50 °C and 1.0 MPa of H<sub>2</sub>.<sup>18</sup> Moreover, Na-containing CeO<sub>2</sub> nanorod-supported Pt catalysts<sup>12</sup> exhibited high yields of aniline and excellent stability for nitrobenzene hydrogenation at room temperature. However, the high cost and scarcity of resources with noble metals limit their industrial applications. Transition metals, including Ni,<sup>19–21</sup> Cu,<sup>22,23</sup> Fe,<sup>24,25</sup> and Co,<sup>26–28</sup> are promising alternatives due to their abundant reserves, low cost, and good catalytic performance under certain conditions. For instance, 10%Ni/r-SiO<sub>2</sub>-CIS<sup>20</sup> illustrated good catalytic activity for nitrobenzene hydrogenation under the reaction condition of 150 °C and 1.0 MPa of H<sub>2</sub>, while Ni@NCQDs<sup>29</sup> achieved high activity (100%) and selectivity (99.8%) for the reduction of *p*-

chloronitrobenzene to *p*-chloroaniline. Ni/CeO<sub>2</sub>-CAS<sup>30</sup> catalysts showed good catalytic performance for the reduction of various nitroarenes under 120 °C and 2.0 MPa of H<sub>2</sub>, and the Co/MA-800<sup>31</sup> nanocatalysts were active for the reductive amination of nitroarenes to obtain imines with high yields of product. To promote the catalytic efficiency of non-noble metal catalysts, formation of a bimetallic structure is a typically used strategy. Due to the synergistic effect between the active metal and the second metal, enhanced hydrogenation performance is achieved. For example, CuNi alloy nanoparticles (NPs) exhibited good performance for catalytic transfer hydrogenation of nitroarene using ethylene glycol as the hydrogen donor,<sup>32</sup> while ceria-supported NiCo alloy catalysts derived from the metal-organic framework<sup>33</sup> demonstrated an aniline yield of 87.9% under 150 °C and 2 MPa of H<sub>2</sub>. NiCu/C@SiO<sub>2</sub>-800<sup>34</sup> catalysts could smoothly transform various substituted nitroaromatics to the corresponding aromatic amines at 120 °C and 2.0 MPa of H<sub>2</sub>, and CoN<sub>x</sub>-Co<sub>y</sub>Zn<sub>s</sub>@NPC catalysts<sup>35</sup> achieved high activity and selectivity, affording almost complete conversions and >98% selectivity in water/methanol mixed solvents. Although the obvious progress of non-noble metal catalysts for hydrogenation of nitroaromatics is achieved, the reaction conditions are still relatively critical, and their catalytic efficiency is required to be further promoted. Specifically, the addition of Co to Ni could promote the

Received: January 5, 2023

Accepted: March 6, 2023

Published: March 20, 2023



hydrogenation of nitroaromatics as mentioned above, and further detailed study of NiCo systems is required to enhance their catalytic efficiency and make the reaction proceed in relatively mild conditions.

In this work, mesoporous silica SBA-16-supported NiCo bimetallic nanocatalysts were prepared by coimpregnation of the precursors followed by calcination and H<sub>2</sub> reduction. Ordered mesoporous materials SBA-16 are selected as supports because of their good thermal stability, large specific surface areas, and pore size,<sup>36</sup> and such three-dimensional ordered networks composed of interconnected pores make the reactants more accessible.<sup>37</sup> In this study, the synthesized catalysts were used for the selective hydrogenation of nitrobenzene and substituted nitroaromatics. Under the reaction conditions of 80 °C, H<sub>2</sub> pressure of 1.0 MPa, and the reaction time of 2.0 h, the yield of aniline over NiCo<sub>0.3</sub>/SBA-16 reaches >99% for nitrobenzene hydrogenation, and the enhanced performance could be ascribed to the synergistic effect between Ni and Co. Studies have reported various bimetallic catalysts with the use of presynthesized bimetallic alloy NPs (organic solvents were used in some cases). Although the use of presynthesized bimetallic alloy NPs could facilitate the understanding of the synergistic effect, their use significantly increases the catalyst preparation cost and hinders their industrial application. In this work, the synergistic effect between Ni and Co enhanced their hydrogenation performance, and the catalysts were prepared by a simple coimpregnation method without organic solvents, which could greatly decrease the cost and have good prospects in industrial applications.

## 2. EXPERIMENTAL SECTION

**2.1. Catalyst Preparation.** Desired amounts of aqueous solutions of 0.8 M Ni(NO<sub>3</sub>)<sub>2</sub>·6H<sub>2</sub>O and 0.8 M Co(NO<sub>3</sub>)<sub>2</sub>·6H<sub>2</sub>O were charged into a glass beaker containing 50 mg of SBA-16. The resultant mixture was magnetically stirred at room temperature for at least 8 h to almost dry. The samples were dried in an oven at 60 °C for 12 h. Then, the dried powders were calcined in air at 300–600 °C for 3 h and further reduced by H<sub>2</sub> at 400–700 °C for 3 h to obtain Ni<sub>x</sub>Co<sub>y</sub>/SBA-16. The real metal loadings were determined by an inductively coupled plasma emission spectrometer (ICP-OES).

**2.2. Catalyst Activity Measurements.** All reactions were carried out in a 25 mL Teflon-lined stainless steel batch reactor with magnetic stirring at 600 rpm. The schematic demonstration of the experimental setup for the reaction is shown in Figure S1. In a typical experiment, 15.0 mL of 75% ethanol, 102 μL of nitrobenzene (1.0 mmol), and 10.0 mg of NiCo<sub>0.3</sub>/SBA-16 (Ni, 25.0 wt %; Co, 8.4 wt %) were charged into the reactor. Then, the reactor was sealed, and residual air in the reactor was removed by hydrogen purging. The hydrogenation reactions were performed under the defined H<sub>2</sub> pressure, reaction temperature, and reaction time. At certain time intervals, the reaction mixture was sampled, filtered, and then analyzed by a gas chromatograph (GC) with a flame ionization detector. The detailed analysis is included in the Supporting Information.

## 3. RESULTS AND DISCUSSION

**3.1. Catalyst Characterization.** Figure 1 shows the X-ray diffraction (XRD) patterns of Ni/SBA-16, Co/SBA-16, and NiCo<sub>0.3</sub>/SBA-16 prepared by calcination at 400 °C and

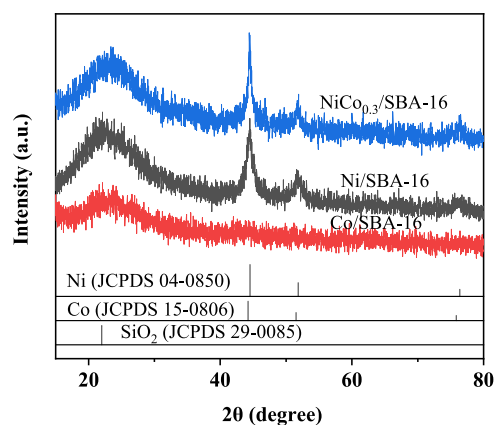


**Figure 1.** XRD patterns of Ni/SBA-16, Co/SBA-16, and NiCo<sub>0.3</sub>/SBA-16. All materials were calcined at 400 °C and subsequently reduced at 600 °C.

subsequent H<sub>2</sub> reduction at 600 °C. All catalysts show a diffraction peak at ~22° 2θ, which is a characteristic peak of SiO<sub>2</sub>. For Ni/SBA-16, three peaks at 44.5, 51.9, and 76.4° were observed, which can be ascribed to the (111), (200), and (220) diffractions of fcc nickel, respectively. However, Co/SBA-16 does not exhibit the characteristic diffractions of Co, possibly due to the formation of amorphous Co. For NiCo<sub>0.3</sub>/SBA-16, three diffractions at 44.4, 51.7, and 76.3° were observed. Since the diffractions of fcc Ni and Co are very close, it is difficult to assign the diffractions of NiCo<sub>0.3</sub>/SBA-16 by XRD measurements (the formation of bimetallic structures of NiCo will be discussed later).

Figure 2 shows the transmission electron microscopy (TEM) images of various materials. A highly ordered arrangement of mesopores in the silica matrix can be clearly observed. As shown in Figure 2a–d, the Ni-containing bimetallic Ni<sub>x</sub>Co<sub>y</sub>/SBA-16 and individual Ni/SBA-16 show distinct NPs in the mesoporous channels and on the surface. In contrast, obvious NPs cannot be observed in the individual Co/SBA-16 (Figure 2e), suggesting the formation of amorphous Co NPs. The absence of obvious metal NPs for Co/SBA-16 is consistent with its XRD patterns in Figure 1, where Co/SBA-16 does not show the characteristic diffractions of metallic Co. Figure S2 presents their corresponding particle size analysis, where the bimetallic Ni<sub>x</sub>Co<sub>y</sub>/SBA-16 and individual Ni/SBA-16 contain ~8 to 9 nm NPs.

Since NiCo<sub>0.3</sub>/SBA-16 showed the best catalytic performance for nitrobenzene hydrogenation, more detailed characterizations were performed for the catalysts. Figure 3 presents the high-angle annular dark-field scanning transition electron microscopy (HAADF-STEM) images of NiCo<sub>0.3</sub>/SBA-16 with energy-dispersive spectroscopy (EDS) phase mappings and line scans. As shown in Figure 3b,c, the Ni and Co elements are highly dispersed on SBA-16, and the combination of Ni and Co phase mappings in Figure 3d confirms that Ni and Co are in close contact. Moreover, the EDS line scans in Figure 3e,f show the copresence of the Ni and Co elements in the selected nanoparticles, confirming the presence of NiCo bimetallic nanostructures.

Figure 4 shows the N<sub>2</sub> adsorption–desorption isotherm and pore size distribution of NiCo<sub>0.3</sub>/SBA-16 at different calcination temperatures, and all tested samples were subsequently reduced by H<sub>2</sub> at 600 °C. As shown in Figure 4a, all tested samples showed type IV N<sub>2</sub> adsorption/

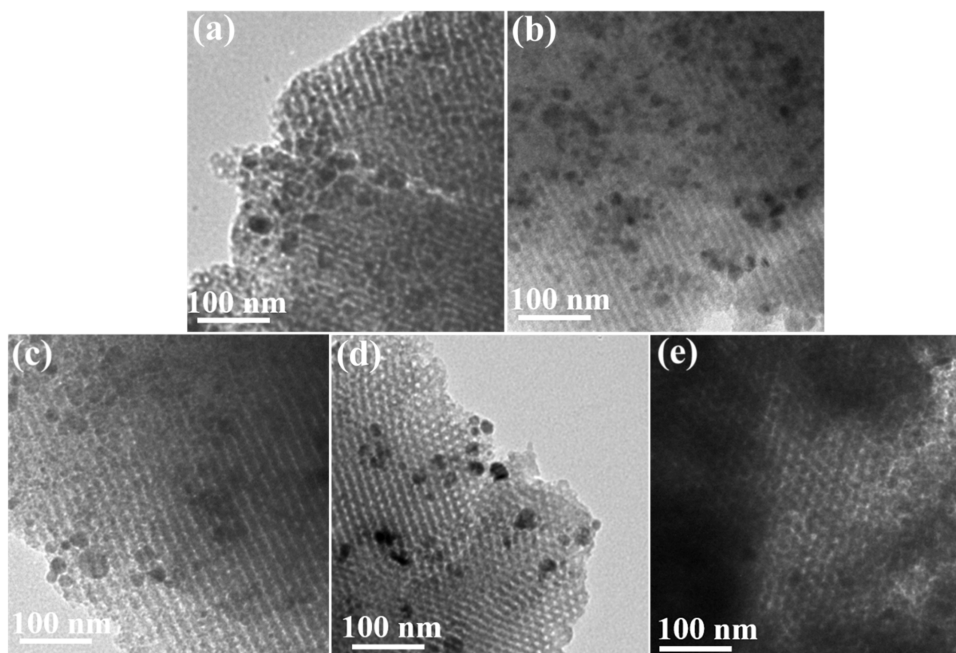


**Figure 2.** TEM images showing (a) NiCo<sub>0.1</sub>/SBA-16, (b) NiCo<sub>0.3</sub>/SBA-16, (c) NiCo<sub>0.5</sub>/SBA-16, (d) Ni/SBA-16, and (e) Co/SBA-16. Calcination at 400 °C and subsequent H<sub>2</sub> reduction at 600 °C were applied to the materials in panels (a)–(e).

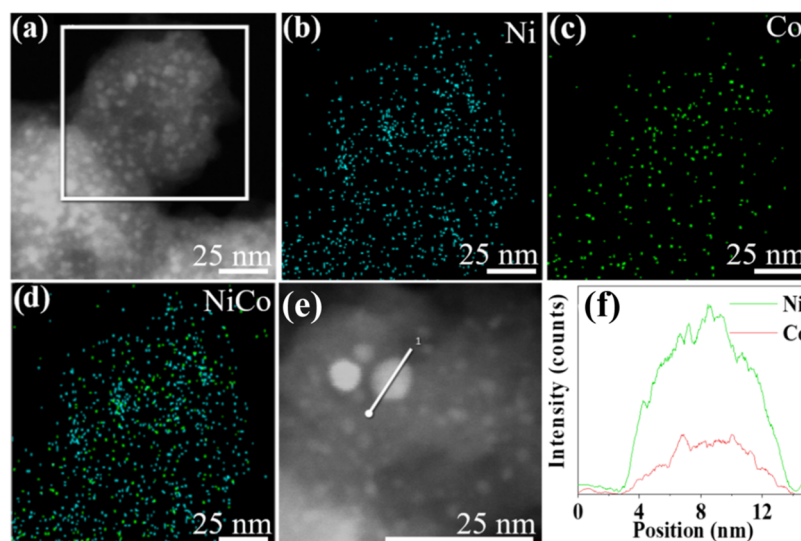


**Figure 3.** (a) HAADF-STEM images of NiCo<sub>0.3</sub>/SBA-16 calcined at 400 °C and subsequently reduced at 600 °C, the inserted square indicating the area for EDS phase mapping; (b) Ni phase mapping; (c) Co phase mapping; (d) the combination of Ni and Co phase mappings; (e) the selected particles for EDS line scans; and (f) the corresponding EDS line scans. The scale bars are 25 nm.

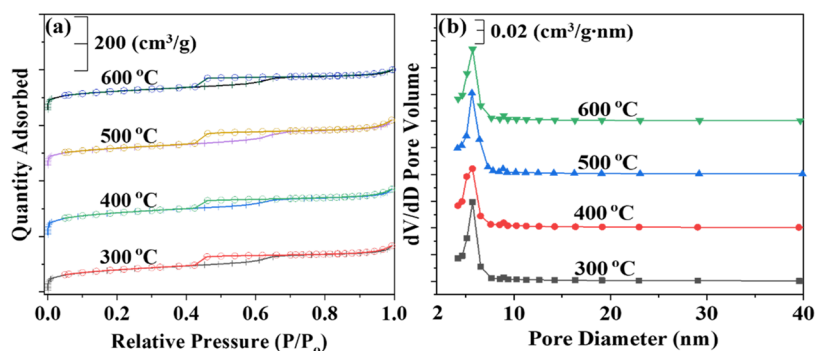
desorption isotherms with hysteresis loops in the relative pressure ( $P/P_0$ ) range from  $\sim 0.4$  to  $\sim 0.7$ , confirming the presence of mesoporous structures in the samples.<sup>38,39</sup> The pore size distributions by the BJH method for these materials are shown in Figure 4b, where the obvious 5–6 nm mesopores are the characteristic mesopores of SBA-16.

Table 1 summarizes the textural properties of NiCo<sub>0.3</sub>/SBA-16 calcined at various temperatures and reduced afterward by H<sub>2</sub> at 600 °C. As shown in Table 1, the BET-specific surface areas of NiCo<sub>0.3</sub>/SBA-16 calcined at 300 and 400 °C are apparently larger than those of NiCo<sub>0.3</sub>/SBA-16 calcined at 500 and 600 °C, and the decrease of BET-specific surface areas is possibly due to pore collapse at higher temperatures. It is mentioned here that the BET-specific surface area of SBA-16 is

700 m<sup>2</sup>/g, and the specific surface areas of all catalysts are significantly lower than that of SBA-16 due to the blockage of mesoporous channels by encapsulation of NPs in the channels.

Since the XRD diffractions of NiCo<sub>0.3</sub>/SBA-16 are very close to those of Ni/SBA-16, X-ray photoelectron spectroscopy (XPS) analysis was used to further investigate the valence states of cobalt element in NiCo<sub>0.3</sub>/SBA-16 calcined at 400 °C and subsequently reduced by H<sub>2</sub> at 600 °C. As shown in Figure S3a, the binding energies at 778.5 and 793.3 eV are ascribed to 2p<sub>3/2</sub> and 2p<sub>1/2</sub> of the Co<sup>0</sup> species, respectively,<sup>40</sup> and the binding energies at 781.9 and 796.9 eV are due to 2p<sub>3/2</sub> and 2p<sub>1/2</sub> of the Co<sup>2+</sup> species.<sup>41</sup> Moreover, the binding energies at 785.4 and 802.0 eV can be assigned to 2p<sub>3/2</sub> satellite and 2p<sub>1/2</sub> satellite of Co<sup>2+</sup> species, respectively.<sup>42</sup> As for the Ni 2p spectra





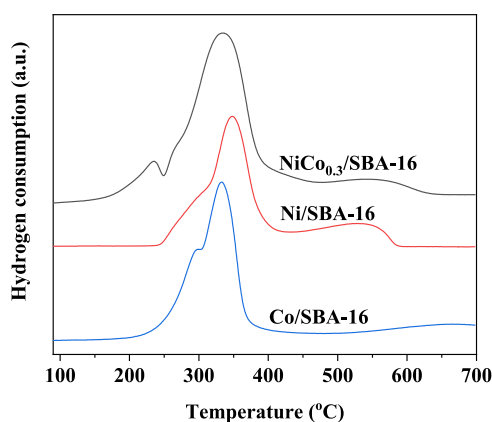
**Figure 4.** (a)  $N_2$  adsorption–desorption isotherms of  $NiCo_{0.3}/SBA-16$  prepared by calcination at various temperatures and subsequent  $H_2$  reduction at  $600\text{ }^\circ\text{C}$ ; and (b) their corresponding pore size distributions by the BJH method.

**Table 1. Textural Properties of  $NiCo_{0.3}/SBA-16$  Prepared by Calcination at Various Temperatures and Subsequent  $H_2$  Reduction at  $600\text{ }^\circ\text{C}$**

samples	$S_{BET}$ ( $m^2/g$ )	pore volume ( $cm^3/g$ )	pore diameter (nm)
$NiCo_{0.3}/SBA-16-300\text{ }^\circ\text{C}$	270	0.22	5.7
$NiCo_{0.3}/SBA-16-400\text{ }^\circ\text{C}$	288	0.23	5.7
$NiCo_{0.3}/SBA-16-500\text{ }^\circ\text{C}$	232	0.22	5.7
$NiCo_{0.3}/SBA-16-600\text{ }^\circ\text{C}$	248	0.21	5.7

in Figure S3b, the binding energies of 853.3 and 870.2 eV can be ascribed to  $2p_{3/2}$  and  $2p_{1/2}$  of the  $Ni^0$  species, respectively, and the binding energies at 856.3 and 874.0 eV can be indexed to  $2p_{3/2}$  and  $2p_{1/2}$  of the  $Ni^{2+}$  species, respectively.<sup>43,44</sup> Moreover, two shake-up satellites (at 862.2 and 880.6 eV)<sup>45</sup> of  $Ni^0$  are also observed in Figure S3b. According to XPS analysis, the molar ratio of  $Ni^0/Ni^{2+}$  is 61.3/38.7, while the ratio of  $Co^0/Co^{2+}$  is 58.5/41.5. The relatively large populations of metal oxides are certainly due to the exposure of the samples to air and the fact that Ni and Co are relatively active metals.

Figure 5 presents the  $H_2$ -TPR profiles of  $NiCo_{0.3}/SBA-16$  and monometallic catalysts calcined at  $400\text{ }^\circ\text{C}$ . As shown in



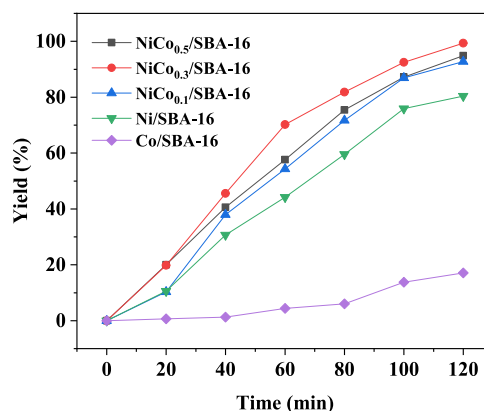
**Figure 5.**  $H_2$ -TPR profiles of  $NiCo_{0.3}/SBA-16$ ,  $Ni/SBA-16$ , and  $Co/SBA-16$ . All materials were calcined at  $400\text{ }^\circ\text{C}$ .

Figure 5, the blue curve of  $Co/SBA-16$  shows a reduction starting from  $\sim 210\text{ }^\circ\text{C}$ , while  $Ni/SBA-16$  illustrates a reduction starting from  $\sim 240\text{ }^\circ\text{C}$ . According to the literature,<sup>46,47</sup> the reduction of Ni oxides usually occurs at relatively higher temperatures. Therefore, the first small peak centered at  $230\text{ }^\circ\text{C}$  in  $NiCo_{0.3}/SBA-16$  (black curve) is similar to that of  $Co/SBA-16$

and can be assigned to the reduction of  $Co_3O_4$  to  $CoO$ .<sup>48</sup> The peak started from  $\sim 250\text{ }^\circ\text{C}$  and ended at  $\sim 450\text{ }^\circ\text{C}$  in  $NiCo_{0.3}/SBA-16$  could be assigned to the reduction of  $Co^{2+}$  species to metallic Co and  $Ni^{2+}$  species to metallic Ni,<sup>46–50</sup> while the peak centered at  $\sim 560\text{ }^\circ\text{C}$  in  $NiCo_{0.3}/SBA-16$  is similar to the peak of  $Ni/SBA-16$  centered at  $\sim 540\text{ }^\circ\text{C}$  and could be ascribed to the reduction of Ni oxides having strong interaction with silica. Based on  $H_2$ -TPR studies, it is concluded that  $H_2$  reduction at  $600\text{ }^\circ\text{C}$  can fully reduce the Ni and Co elements to facilitate the formation of the alloy phase.

**3.2. Catalytic Hydrogenation of Nitrobenzene.** The hydrogenation of nitrobenzene is carried out in organic solvents at defined temperatures and hydrogen pressures. The actual metal loadings of different  $Ni_xCo_y/SBA-16$  determined by ICP-OES are shown in Table S1. To ensure the same molar ratio of nitrobenzene/(Ni+Co), different weights of catalysts were used due to the different loadings of Ni and Co.

The effect of different ratios of Ni/Co of  $Ni_xCo_y/SBA-16$  on the hydrogenation of nitrobenzene is shown in Figure 6. In this reaction, the selectivity of aniline is nearly 100%, so its yield is basically equal to the conversion of nitrobenzene. As shown in Figure 6, under the same reaction conditions, individual  $Co/SBA-16$  catalysts do not show significant activity for the hydrogenation of nitrobenzene. In contrast, individual  $Ni/SBA-16$  catalysts are more active for this reaction, showing a



**Figure 6.** Effect of the Ni/Co molar ratios on aniline yields over  $Ni_xCo_y/SBA-16$ . All catalysts were calcined at  $400\text{ }^\circ\text{C}$  and reduced by  $H_2$  at  $600\text{ }^\circ\text{C}$ . Reaction conditions: nitrobenzene, 1.0 mmol; nitrobenzene/(Ni+Co) molar ratio, 24/1; solvents, 15.0 mL of 75% ethanol;  $H_2$ , 1.0 MPa; reaction temperature,  $80\text{ }^\circ\text{C}$ ; and speed of agitation, 600 rpm.

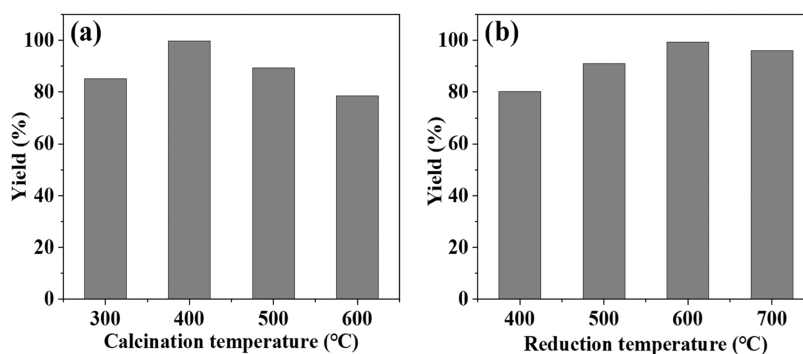


**Figure 7.** Effects of (a) calcination temperatures and (b) reduction temperatures of NiCo<sub>0.3</sub>/SBA-16 on aniline yields for nitrobenzene hydrogenation. H<sub>2</sub> reduction at 600 °C for panel (a) and calcination at 400 °C for panel (b). Reaction conditions: nitrobenzene, 1.0 mmol; nitrobenzene/(Ni+Co) ratio, 24/1; solvents, 15.0 mL of 75% ethanol; H<sub>2</sub>, 1.0 MPa; reaction temperature, 80 °C; reaction time, 2.0 h; and speed of agitation, 600 rpm.

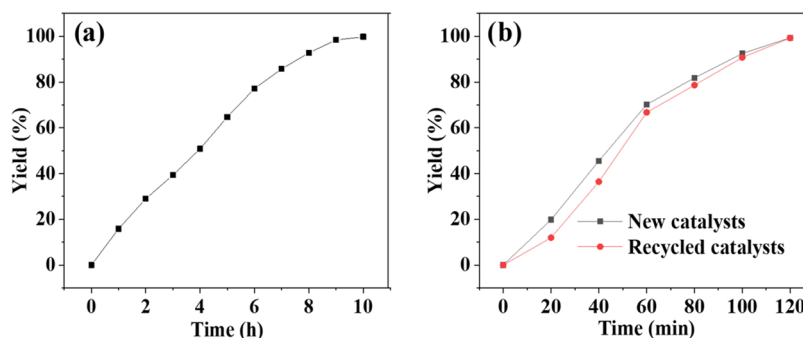


**Figure 8.** (a) Nitrobenzene hydrogenation over NiCo<sub>0.3</sub>/SBA-16 at a high nitrobenzene/(Ni+Co) ratio of 120/1; (b) nitrobenzene hydrogenation over the recovered NiCo<sub>0.3</sub>/SBA-16 at a nitrobenzene/(Ni+Co) ratio of 24/1. Reaction conditions: nitrobenzene, 5.0 mmol for panel (a) and 1.0 mmol for panel (b); solvents, 15.0 mL of 75% ethanol; H<sub>2</sub>, 1.0 MPa; reaction temperature, 80 °C; and speed of agitation, 600 rpm. The catalysts were calcined at 400 °C and reduced by H<sub>2</sub> at 600 °C.

yield of 80% at 2.0 h. After the addition of Co by retaining the same moles of (Ni+Co) in catalytic reactions, all of the studied Ni<sub>x</sub>Co<sub>y</sub>/SBA-16 show higher activities than that of individual Ni/SBA-16. When the Co/Ni ratios reach 1/0.3, the best performance was achieved, showing an aniline yield of 99.8% at 2.0 h. The enhancement is possibly due to the synergistic effect between Ni and Co. Further increasing the Co/Ni ratios to 0.5/1 causes a slight decrease in aniline yield to 92% at 2.0 h possibly due to the dilution of the Ni surface by excessive Co atoms. Based on the above results, NiCo<sub>0.3</sub>/SBA-16 was used for further studies.

Figure 7a shows the catalytic activity of NiCo<sub>0.3</sub>/SBA-16 at different calcination temperatures, where all catalysts were reduced at 600 °C. As shown in Figure 7a, the yields at 2.0 h increase from 85.2% at 300 °C to 99.8% at 400 °C. With a further increase of the calcination temperatures, the yield decreased obviously, showing 89.4% at 500 °C and 78.5% at 600 °C. The poor catalytic performance at 300 °C may be due to the incomplete removal of nitrate. The decrease in the catalytic performance of NiCo<sub>0.3</sub>/SBA-16 with calcination at temperatures above 400 °C is mainly due to the decrease of specific surface areas at higher calcination temperatures (Table 1).

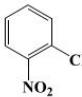
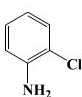
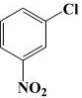
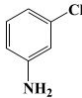
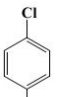
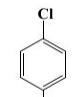
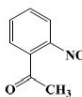
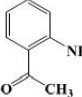
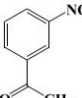
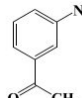
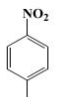
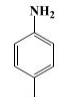
Figure 7b presents the catalytic activity of NiCo<sub>0.3</sub>/SBA-16 at different reduction temperatures, where all catalysts were calcined at 400 °C before reduction. As shown in Figure 7b, the yields increase from 80.1% at 400 °C to 90.1% at 500 °C and reach the best performance of 99.8% at 600 °C. Further increasing the reduction temperatures to 700 °C causes the

aniline yield to slightly decrease to 95.9%. Based on the H<sub>2</sub>-TPR results in Figure 5, we speculate that the relatively worse performance at the reduction temperatures ≤500 °C can be ascribed to the incomplete reduction of metal oxides and the less formation of NiCo bimetallic nanostructures.

Figure S4 illustrates the influence of solvents on the catalytic performance of NiCo<sub>0.3</sub>/SBA-16. As shown in Figure S4, using methanol, isopropanol, and ethanol as solvents only give the aniline yields ≤23.8% at 2.0 h. When water is used as the solvent, the aniline yields are greatly improved to 89.7%. When 75% ethanol is used as the solvent, the yields are further enhanced to 99.8% at 2.0 h. According to the literature,<sup>51,52</sup> the improvement of catalytic performance is mainly attributed to the competitive adsorption of water and ethanol on the surface active sites and the intermolecular interactions between water and reactant or product molecules. The use of ethanol and water-mixed solvents is conducive to the adsorption of nitrobenzene and the desorption of aniline by increasing the concentration of adsorbed nitrobenzene and reducing the concentration of adsorbed aniline, thus accelerating the catalytic reactions.<sup>52</sup>

Figure S5 shows the effects of reaction temperatures and hydrogen pressures on aniline yields over NiCo<sub>0.3</sub>/SBA-16. As shown in Figure S5a, the yields of aniline increase significantly as the temperatures increase from 60 to 120 °C. When the reaction temperature is ≥80 °C, the yields of aniline at 2.0 h approach >99%. As shown in Figure S5b, the H<sub>2</sub> pressures have an obvious influence on the reaction, especially in the

Table 2. Catalytic Hydrogenation of Various Substituted Nitroaromatics over Ni/SBA-16 and NiCo<sub>0.3</sub>/SBA-16<sup>a</sup>

Reactants	Main products	Time (h)	Cat.	Conv. (%)	Sel. (%)
		3.0	Ni/SBA-16	74.2	86.7
		3.0	NiCo <sub>0.3</sub> /SBA-16	95.6	89.5
		3.5	Ni/SBA-16	72.2	99.5
		3.5	NiCo <sub>0.3</sub> /SBA-16	96.1	100.0
		3.0	Ni/SBA-16	75.5	94.3
		3.0	NiCo <sub>0.3</sub> /SBA-16	98.7	95.9
		2.0	Ni/SBA-16	81.4	44.8
		2.0	NiCo <sub>0.3</sub> /SBA-16	97.8	76.7
		5.0	Ni/SBA-16	65.8	95.3
		5.0	NiCo <sub>0.3</sub> /SBA-16	90.4	99.6
		4.0	Ni/SBA-16	82.1	89.9
		4.0	NiCo <sub>0.3</sub> /SBA-16	91.6	97.2

<sup>a</sup>Reaction conditions: reactants, 1.0 mmol; reactants/(Ni+Co) ratio, 24/1; solvents, 15.0 mL of 75% ethanol; H<sub>2</sub>, 1.0 MPa; reaction temperature, 80 °C; and speed of agitation, 600 rpm.

early stage of the reactions, but the aniline yields at 2.0 h could reach > 99% for H<sub>2</sub> pressures ≥0.5 MPa.

Figure 8 presents the catalytic stability of NiCo<sub>0.3</sub>/SBA-16 for the hydrogenation of nitrobenzene. It is difficult to recover catalysts in the autoclave system, and a significant percentage of catalysts are lost during cycle-to-cycle experiments. Therefore, the stability test was performed in the nitrobenzene/(Ni+Co) molar ratio as high as 120/1, which is 5 times higher than the normal test. After the above test with a nitrobenzene/(Ni+Co) molar ratio of 120/1, the solids were collected, washed, and dried for a normal test with a nitrobenzene/(Ni+Co) molar ratio of 24/1. The total amount of reactants in this work is equal to the sum of the amounts of reactants during six cycles of normal experiments, and the reaction time is also equal to the total reaction time of six cycle experiments. As shown in Figure 8a, the hydrogenation reaction with a nitrobenzene/(Ni+Co) molar ratio of 120/1 achieves a 99.8% yield in 10.0 h, showing nearly the same catalytic efficiency at a high dosage of reactants as that of a normal test. In a reaction with high dosages of reactants, the metals in the catalysts may leach into the solution but still play the catalytic role. Therefore, after the mentioned reaction, the catalysts were recovered and further performed at the normal reaction conditions for comparison. Figure 8b shows the reaction curve with the recovered catalyst with a nitrobenzene/(Ni+Co) molar ratio of 24/1. After treating the reactants five times, the recovered NiCo<sub>0.3</sub>/SBA-16 exhibits almost the same perform-

ance as the fresh catalysts, showing excellent catalytic stability. Figure S6a presents the TEM image of the used catalysts, while Figure S6b shows the corresponding size distributions. Although no obvious change was observed in the TEM images (Figure S6a), the particle size of NiCo<sub>0.3</sub>/SBA-16 slightly increased from 8.2 nm for the fresh catalysts to 9.1 nm for the used catalysts, which may be responsible for the small decrease of aniline yields observed in Figure 8b.

We further extended the application of NiCo<sub>0.3</sub>/SBA-16 catalysts to hydrogenation of various substituted nitroaromatics. As shown in Table 2, hydrogenation of nitrobenzenes with different groups (carbonyl and chloride) at different substitutions (*o*-, *m*-, and *p*-) was investigated. For hydrogenation of *o*-, *m*- and *p*-chloronitrobenzene (CNB), NiCo<sub>0.3</sub>/SBA-16 shows significantly higher conversions than the control Ni/SBA-16. The *o*-, *m*-, and *p*-CNB conversions over NiCo<sub>0.3</sub>/SBA-16 were 95.6, 96.1, and 98.7%, respectively, while the conversions over Ni/SBA-16 were 74.2, 72.2, and 75.5%, respectively. The main byproduct for CNB hydrogenation is aniline, which is produced by hydrodechlorination of CNB. For hydrogenation of *o*-, *m*-, and *p*-nitroacetophenone (NAP), NiCo<sub>0.3</sub>/SBA-16 shows significantly enhanced conversions and selectivity relative to Ni/SBA-16. For example, 97.8% of *o*-NAP conversion and 76.7% of *o*-acetylaniline selectivity are achieved with NiCo<sub>0.3</sub>/SBA-16, while those over Ni/SBA-16 are 81.4% and 44.8%, respectively. The main byproducts for nitroacetophenone hydrogenation are relatively

complex. According to the literature,<sup>53</sup> aminophenyl ethanol, aminocyclohexyl ethanol, and ethylaniline are the possible main byproducts. In this study, NiCo<sub>0.3</sub>/SBA-16 catalysts demonstrate enhanced catalytic properties for all six substrates, indicating good adaptability.

Table S2 presents the comparison of catalytic performance between different transition metal-based catalysts for nitrobenzene hydrogenation. As shown in Table S2, the hydrogenation of nitrobenzene over NiCo<sub>0.3</sub>/SBA-16 can proceed at relatively mild reaction conditions. The catalytic enhancement is ascribed to the synergistic effect between Ni and Co, where the formation of bimetallic nanostructures could change the coordination behaviors of reactants and intermediates, thus promoting their hydrogenation performance. Moreover, the NiCo<sub>0.3</sub>/SBA-16 was prepared by a simple coimpregnation method with a relatively low preparation cost, making them suitable for industrial applications.

#### 4. CONCLUSIONS

In summary, bimetallic NiCo<sub>0.3</sub>/SBA-16 catalysts were prepared by the coimpregnation method and used to catalyze the hydrogenation of nitroaromatic to aminoaromatics. Compared with monometallic Ni/SBA-16, the catalytic performance of NiCo<sub>0.3</sub>/SBA-16 for a series of substituted nitrobenzenes was improved. The formation of bimetallic nanostructures not only enhances their catalytic activities but also improves their catalytic selectivity. The enhanced catalytic performance can be attributed to the interaction between Ni and Co. We believe that the simple and inexpensive synthetic method used in this work can extend to prepare other bimetallic catalysts to enhance their catalytic performance, and such a simple method can facilitate the industrial applications of bimetallic catalysts.

#### ■ ASSOCIATED CONTENT

##### SI Supporting Information

The Supporting Information is available free of charge at <https://pubs.acs.org/doi/10.1021/acsomega.3c00076>.

Chemicals, catalyst characterization, GC analysis method, schematic demonstration of the experimental set-up, particle size histograms, XPS spectra, effects of solvents, reaction temperatures, and H<sub>2</sub> pressures on catalytic performance, and post-characterization of the used catalysts (PDF)

#### ■ AUTHOR INFORMATION

##### Corresponding Author

Shenghu Zhou – Shanghai Key Laboratory of Multiphase Materials Chemical Engineering, School of Chemical Engineering, East China University of Science and Technology, Shanghai 200237, P. R. China; [orcid.org/0000-0002-8203-6546](https://orcid.org/0000-0002-8203-6546); Email: [zhoushenghu@ecust.edu.cn](mailto:zhoushenghu@ecust.edu.cn); Fax: (+86) 21-64253159

##### Authors

Jiajuan Li – Shanghai Key Laboratory of Multiphase Materials Chemical Engineering, School of Chemical Engineering, East China University of Science and Technology, Shanghai 200237, P. R. China

Zizhu Wang – Shanghai Key Laboratory of Multiphase Materials Chemical Engineering, School of Chemical

Engineering, East China University of Science and Technology, Shanghai 200237, P. R. China

Yirui Ma – Shanghai Key Laboratory of Multiphase Materials Chemical Engineering, School of Chemical Engineering, East China University of Science and Technology, Shanghai 200237, P. R. China

Caiyun Xu – Shanghai Key Laboratory of Multiphase Materials Chemical Engineering, School of Chemical Engineering, East China University of Science and Technology, Shanghai 200237, P. R. China

Complete contact information is available at:

<https://pubs.acs.org/10.1021/acsomega.3c00076>

#### Notes

The authors declare no competing financial interest.

#### ■ ACKNOWLEDGMENTS

This work is financially supported by the National Natural Science Foundation of China (Grant Nos. 22078099 and 21776090).

#### ■ REFERENCES

- (1) Song, J.; Huang, Z.; Pan, L.; Li, K.; Zhang, X.; Wang, L.; Zou, J. Review on Selective Hydrogenation of Nitroarene by Catalytic, Photocatalytic and Electrocatalytic Reactions. *Appl. Catal., B* **2018**, *227*, 386–408.
- (2) Makosch, M.; Sá, J.; Kartusch, C.; Richner, G.; Bokhoven, J.; Hungerbühler, K. Hydrogenation of Nitrobenzene over Au/MeO<sub>x</sub> Catalysts—A Matter of the Support. *ChemCatChem* **2012**, *4*, 59–63.
- (3) Yu, H.; Wu, C.; Wang, S.; Li, T.; Yin, H. Transition Metal Oxide-modified Ir Nanoparticles Supported on SBA-15 Silica for Selective Hydrogenation of Substituted Nitroaromatics. *ACS Appl. Nano Mater.* **2021**, *4*, 7213–7220.
- (4) Hao, C.-H.; Guo, X.; Sankar, M.; Yang, H.; Ma, B.; Zhang, Y.; Tong, X.; Jin, G.; Guo, X. Synergistic Effect of Segregated Pd and Au Nanoparticles on Semiconducting SiC for Efficient Photocatalytic Hydrogenation of Nitroarenes. *ACS Appl. Mater. Interfaces* **2018**, *10*, 23029–23036.
- (5) Benz, M.; Prins, R. Kinetics of the Reduction of Aromatic Nitro Compounds with Hydrazine Hydrate in the Presence of An Iron Oxide Hydroxide Catalyst. *Appl. Catal., A* **1999**, *183*, 325–333.
- (6) Lauwiner, M.; Rys, P.; Wissmann, J. Reduction of Aromatic Nitro Compounds with Hydrazine Hydrate in the Presence of An Iron Oxide Hydroxide Catalyst. I. The Reduction of Monosubstituted Nitrobenzenes with Hydrazine Hydrate in the Presence of Ferrihydrite. *Appl. Catal., A* **1998**, *172*, 141–148.
- (7) Downing, R.; Kunkeler, P.; Bekkum, H. Catalytic Syntheses of Aromatic Amines. *Catal. Today* **1997**, *37*, 121–136.
- (8) Westerhaus, F. A.; Jagadeesh, R.; Wienhöfer, G.; Pohl, M.; Radnik, J.; Surkus, A.; Rabeah, J.; Junge, K.; Junge, H.; Nielsen, M.; Brückner, A.; Beller, M. Heterogenized Cobalt Oxide Catalysts for Nitroarene Reduction by Pyrolysis of Molecularly Defined Complexes. *Nat. Chem.* **2013**, *5*, 537–543.
- (9) Couto, C. S.; Madeira, L.; Nunes, C.; Araújo, P. Liquid-Phase Hydrogenation of Nitrobenzene in a Tubular Reactor: Parametric Study of the Operating Conditions Influence. *Ind. Eng. Chem. Res.* **2017**, *56*, 3231–3242.
- (10) Cárdenas-Lizana, F.; Hao, Y.; Crespo-Quesada, M.; Yuranov, I.; Wang, X.; Keane, M.; Kiwi-Minsker, L. Selective Gas Phase Hydrogenation of *p*-Chloronitrobenzene over Pd Catalysts: Role of the Support. *ACS Catal.* **2013**, *3*, 1386–1396.
- (11) Cárdenas-Lizana, F.; Gómez-Quero, S.; Jacobs, G.; Ji, Y.; Davis, B.; Kiwi-Minsker, L.; Keane, M. Alumina Supported Au–Ni: Surface Synergism in the Gas Phase Hydrogenation of Nitro-Compounds. *J. Phys. Chem. C* **2012**, *116*, 11166–11180.



- (12) Zhang, Q.; Bu, J.; Wang, J.; Sun, C.; Zhao, D.; Sheng, G.; Xie, X.; Sun, M.; Yu, I. Highly Efficient Hydrogenation of Nitrobenzene to Aniline over Pt/CeO<sub>2</sub> Catalysts: The Shape Effect of the Support and Key Role of Additional Ce<sup>3+</sup> Sites. *ACS Catal.* **2020**, *10*, 10350–10363.
- (13) Liu, H.; Yu, H.; Xiong, C.; Zhou, S. Architecture Controlled PtNi@mSiO<sub>2</sub> and Pt–NiO@mSiO<sub>2</sub> Mesoporous Core–Shell Nanocatalysts for Enhanced *p*-Chloronitrobenzene Hydrogenation Selectivity. *RSC Adv.* **2015**, *5*, 20238–20247.
- (14) Yu, X.; Wang, M.; Li, H. Study on the Nitrobenzene Hydrogenation over a Pd-B/SiO<sub>2</sub> Amorphous Catalyst. *Appl. Catal., A* **2000**, *202*, 17–22.
- (15) Lyu, J.; Wang, J.; Lu, C.; Ma, L.; Zhang, Q.; He, X.; Li, X. Size-Dependent Halogenated Nitrobenzene Hydrogenation Selectivity of Pd Nanoparticles. *J. Phys. Chem. C* **2014**, *118*, 2594–2601.
- (16) Currall, K.; Jackson, S. Hydrogenation of 4-Nitroacetophenone over Rh/Silica. *Appl. Catal., A* **2014**, *484*, 59–63.
- (17) Xu, C.; Li, Q.; Zhang, Q.; Li, K.; Yin, H.; Zhou, S. Structural Identification and Enhanced Catalytic Performance of Alumina-Supported Well-Defined Rh–SnO<sub>2</sub> Close-Contact Heteroaggregate Nanostructures. *ACS Appl. Nano Mater.* **2019**, *2*, 5086–5095.
- (18) Wang, J.; Du, C.; Wei, Q.; Shen, W. Two-Dimensional Pd Nanosheets with Enhanced Catalytic Activity for Selective Hydrogenation of Nitrobenzene to Aniline. *Energy Fuels* **2021**, *35*, 4358–4366.
- (19) Meng, X.; Cheng, H.; Akiyama, Y.; Hao, Y.; Qiao, W.; Yu, Y.; Zhao, F.; Fujita, S.; Arai, M. Selective Hydrogenation of Nitrobenzene to Aniline in Dense Phase Carbon Dioxide over Ni/ $\gamma$ -Al<sub>2</sub>O<sub>3</sub>: Significance of Molecular Interactions. *J. Catal.* **2009**, *264*, 1–10.
- (20) Xie, Z.; Zhang, T.; Zhao, Z. Ni Nanoparticles Grown on SiO<sub>2</sub> Supports Using a Carbon Interlayer Sacrificial Strategy for Chemoselective Hydrogenation of Nitrobenzene and *m*-Cresol. *ACS Appl. Nano Mater.* **2021**, *4*, 9353–9360.
- (21) Ma, C.; Liu, W.; Duan, X.; Zhang, C.; Sang, L.; Zhang, J. Preparation of Highly Effective Ni Foam Monolithic Catalysts by Electrolytic Deposition for Nitrobenzene Hydrogenation in a Micropacked Bed. *Ind. Eng. Chem. Res.* **2022**, *61*, 11276–11287.
- (22) Sithisa, S.; Sooknoi, T.; Ma, Y.; Balbuena, P.; Resasco, D. Kinetics and Mechanism of Hydrogenation of Furfural on Cu/SiO<sub>2</sub> Catalysts. *J. Catal.* **2011**, *277*, 1–13.
- (23) Liu, H.; Li, X.; Ma, Z.; Sun, M.; Li, M.; Zhang, Z.; Zhang, L.; Tang, Z.; Yao, Y.; Huang, B.; Guo, S. Atomically Dispersed Cu Catalyst for Efficient Chemoselective Hydrogenation Reaction. *Nano Lett.* **2021**, *21*, 10284–10291.
- (24) Yun, R.; Zhan, F.; Li, N.; Zhang, B.; Ma, W.; Hong, L.; Sheng, T.; Du, L.; Zheng, B.; Liu, S. Fe Single Atoms and Fe<sub>2</sub>O<sub>3</sub> Clusters Liberated from N-Doped Polyhedral Carbon for Chemoselective Hydrogenation Under Mild Conditions. *ACS Appl. Mater. Interfaces* **2020**, *12*, 34122–34129.
- (25) Yun, R.; Zhang, S.; Ma, W.; Lv, X.; Liu, S.; Sheng, T.; Wang, S. Fe/Fe<sub>3</sub>C Encapsulated in N-Doped Carbon Tubes: A Recyclable Catalyst for Hydrogenation with High Selectivity. *Inorg. Chem.* **2019**, *58*, 9469–9475.
- (26) Xu, Y.; Shan, W.; Liang, X.; Gao, X.; Li, W.; Li, H.; Qiu, X. Cobalt Nanoparticles Encapsulated in Nitrogen-Doped Carbon Shells: Efficient and Stable Catalyst for Nitrobenzene Reduction. *Ind. Eng. Chem. Res.* **2020**, *59*, 4367–4376.
- (27) Chen, P.; Yang, F.; Kostka, A.; Xia, W. Interaction of Cobalt Nanoparticles with Oxygen- and Nitrogen-Functionalized Carbon Nanotubes and Impact on Nitrobenzene Hydrogenation Catalysis. *ACS Catal.* **2014**, *4*, 1478–1486.
- (28) Liu, K.; Cao, Y.; Yang, S.; Wu, C.; Zhang, Z.; Zhang, Q.; Zhang, H. Molybdenum Carbide-Promoted Cobalt as an Efficient Catalyst for Selective Hydrogenation. *Ind. Eng. Chem. Res.* **2020**, *59*, 14267–14277.
- (29) Ma, C.; Zhou, Y.; Yan, W.; He, W.; Liu, Q.; Li, Z.; Wang, H.; Li, G.; Yang, Y.; Han, W.; Lu, C.; Li, X. Predominant Catalytic Performance of Nickel Nanoparticles Embedded into Nitrogen-Doped Carbon Quantum Dot-Based Nanosheets for the Nitro-reduction of Halogenated Nitrobenzene. *ACS Sustainable Chem. Eng.* **2022**, *10*, 8162–8171.
- (30) She, W.; Qi, T.; Cui, M.; Yan, P.; Weng Ng, S.; Li, W.; Li, M. High Catalytic Performance of a CeO<sub>2</sub>-Supported Ni Catalyst for Hydrogenation of Nitroarenes, Fabricated via Coordination-Assisted Strategy. *ACS Appl. Mater. Interfaces* **2018**, *10*, 14698–14707.
- (31) Goyal, V.; Sarki, N.; Singh, B.; Ray, A.; Poddar, M.; Bordoloi, A.; Narani, A.; Natte, K. Carbon-Supported Cobalt Nanoparticles as Catalysts for the Selective Hydrogenation of Nitroarenes to Arylamines and Pharmaceuticals. *ACS Appl. Nano Mater.* **2020**, *3*, 11070–11079.
- (32) Shi, H.; Dai, X.; Liu, Q.; Zhang, T.; Zhang, Y.; Shi, Y.; Wang, T. Magnetic CuNi Alloy Nanoparticles for Catalytic Transfer Hydrogenation of Nitroarene. *Ind. Eng. Chem. Res.* **2021**, *60*, 16011–16022.
- (33) Li, W.; She, W.; Wang, J.; Li, X.; Li, J.; Shi, J.; Li, G. Metal–Organic Framework-Derived Ceria-Supported Ni–Co Alloy Nanocatalysts for Hydrogenation of Nitroarenes. *ACS Appl. Nano Mater.* **2020**, *3*, 10796–10804.
- (34) Sheng, Y.; Lin, X.; Yue, S.; Liu, Y.; Zou, X.; Wang, X.; Lu, X. Highly Efficient non-Noble Metallic NiCu Nanoalloy Catalysts for Hydrogenation of Nitroarenes. *Mater. Adv.* **2021**, *2*, 6722.
- (35) Zhang, G.; Tang, F.; Wang, X.; An, P.; Wang, L.; Liu, Y. Co, N-Codoped Porous Carbon-Supported Co<sub>2</sub>ZnS with Superior Activity for Nitroarene Hydrogenation. *ACS Sustainable Chem. Eng.* **2020**, *8*, 6118–6126.
- (36) Ganji, S.; Bukya, P.; Liu, Z.; Rao, K.; Burri, D. A Carboxylic Acid Functionalized SBA-15 Supported Pd Nanocatalyst: An Efficient Catalyst for Hydrogenation of Nitrobenzene to Aniline in water. *New J. Chem.* **2019**, *43*, 11871–11875.
- (37) Zheng, P.; Hu, D.; Meng, Q.; Liu, C.; Wang, X.; Fan, J.; Duan, A.; Xu, C. Influence of Support Acidity on the HDS Performance over  $\beta$ -SBA-16 and Al-SBA-16 Substrates: A Combined Experimental and Theoretical Study. *Energy Fuels* **2019**, *33*, 1479–1488.
- (38) Zhang, S.; Muratsugu, S.; Ishiguro, N.; Tada, M. Ceria-Doped Ni/SBA-16 Catalysts for Dry Reforming of Methane. *ACS Catal.* **2013**, *3*, 1855–1864.
- (39) Ravikovitch, P. I.; Neimark, A. Density Functional Theory of Adsorption in Spherical Cavities and Pore Size Characterization of Templated Nanoporous Silicas with Cubic and Three-Dimensional Hexagonal Structures. *Langmuir* **2002**, *18*, 1550–1560.
- (40) Dufresne, P.; Payen, E.; Grmlblot, J.; Bonnelle, J. Study of Ni–Mo- $\gamma$ -Al<sub>2</sub>O<sub>3</sub> Catalysts by X-Ray Photoelectron and Raman Spectroscopy. Comparison with Co–Mo- $\gamma$ -Al<sub>2</sub>O<sub>3</sub> Catalysts. *J. Phys. Chem. A* **1981**, *85*, 2344–2351.
- (41) Wu, L.-K.; Wu, W.; Xia, J.; Cao, H.; Hou, G.; Tang, Y.; Zheng, G. A Nanostructured Nickel–Cobalt Alloy with an Oxide Layer for an Efficient oxygen Evolution Reaction. *J. Mater. Chem. A* **2017**, *5*, 10669–10677.
- (42) Peng, Y.; Wang, L.; Liu, Y.; Chen, H.; Lei, J.; Zhang, J. Visible-Light-Driven Photocatalytic H<sub>2</sub>O<sub>2</sub> Production on g-C<sub>3</sub>N<sub>4</sub> Loaded with CoP as a Noble Metal Free Cocatalyst. *Eur. J. Inorg. Chem.* **2017**, *2017*, 4797–4802.
- (43) Wang, R.; Chu, C.; Hu, T.; Dong, Y.; Guo, C.; Sheng, X.; Lin, P.; Chung, C.; Chu, P. Surface XPS Characterization of NiTi Shape Memory Alloy after Advanced Oxidation Processes in UV/H<sub>2</sub>O<sub>2</sub> Photocatalytic System. *Appl. Surf. Sci.* **2007**, *253*, 8507–8512.
- (44) Wang, H.; Li, X.; Lan, X.; Wang, T. Supported Ultrafine NiCo Bimetallic Alloy Nanoparticles Derived from Bimetal–Organic Frameworks: A Highly Active Catalyst for Furfuryl Alcohol Hydrogenation. *ACS Catal.* **2018**, *8*, 2121–2128.
- (45) Gopi, S.; Selvamani, V.; Yun, K. MoS<sub>2</sub> Decoration Followed by P Inclusion over Ni–Co Bimetallic Metal–Organic Framework-Derived Heterostructures for Water Splitting. *Inorg. Chem.* **2021**, *60*, 10772–10780.
- (46) Wang, F.; Han, K.; Xu, L.; Yu, H.; Shi, W. Ni/SiO<sub>2</sub> Catalyst Prepared by Strong Electrostatic Adsorption for a Low-Temperature Methane Dry Reforming Reaction. *Ind. Eng. Chem. Res.* **2021**, *60*, 3324–3333.



(47) Bai, Y.; Qiu, X.; Zhang, Q.; Qiu, S.; Qin, Y.; Wang, T. Green Synthesis of Highly Dispersed Ni/SiO<sub>2</sub> Catalysts Using Natural Biomass of Sesbania Powder. *Ind. Eng. Chem. Res.* **2020**, *59*, 17399–17407.

(48) Bambal, A. S.; Kugler, E.; Gardner, T.; Dadyburjor, D. Effect of Surface Modification by Chelating Agents on Fischer–Tropsch Performance of Co/SiO<sub>2</sub> Catalysts. *Ind. Eng. Chem. Res.* **2013**, *52*, 16675–16688.

(49) Zhao, B.; Liu, P.; Li, S.; Shi, H.; Jia, X.; Wang, Q.; Yang, F.; Song, Z.; Guo, C.; Hu, J.; Chen, Z.; Yan, X.; Ma, X. Bimetallic Ni-Co Nanoparticles on SiO<sub>2</sub> as Robust Catalyst for CO Methanation: Effect of Homogeneity of Ni-Co Alloy. *Appl. Catal., B* **2020**, *278*, No. 119307.

(50) Jia, C.; Dai, Y.; Yang, Y.; Chew, J. Nickel-Cobalt Catalyst Supported on TiO<sub>2</sub>-Coated SiO<sub>2</sub> Spheres for CO<sub>2</sub> Methanation in a Fluidized Bed. *Int. J. Hydrogen Energy* **2019**, *44*, 13443–13455.

(51) Akpa, B.; D'Agostino, C.; Gladden, L.; Hindle, K.; Manyar, H.; McGregor, J.; Li, R.; Neurock, M.; Sinha, N.; Stitt, E.; Weber, D.; Zeitler, J.; Rooney, D. Solvent Effects in the Hydrogenation of 2-Butanone. *J. Catal.* **2012**, *289*, 30–41.

(52) Wang, H.; Wang, Y.; Li, Y.; Lan, X.; Ali, B.; Wang, T. Highly Efficient Hydrogenation of Nitroarenes by N-Doped Carbon-Supported Cobalt Single-Atom Catalyst in Ethanol/Water Mixed Solvent. *ACS Appl. Mater. Interfaces* **2020**, *12*, 34021–34031.

(53) Abdul-Wahab, M. I.; Jackson, S. Hydrogenation of 3-Nitroacetophenone over Rhodium/Silica Catalysts: Effect of Metal Dispersion and Catalyst Support. *Appl. Catal., A* **2013**, *462–463*, 121–128.